Critical Behavior and Scaling Relationships at the SmA_d−N and N−I Transitions in Nonyloxycyanobiphenyl (9OCB)

P. Cusmin,[†] M. R. de la Fuente,[‡] J. Salud,[†] M. A. Pérez-Jubindo,[‡] S. Diez-Berart,[†] and D. O. López*,[†]

Laboratori de Caracterització de Materials (LCM), Departament de Física i Enginyeria Nuclear, ETSEIB, Universitat Politècnica de Catalunya, Diagonal 647, 08028 Barcelona, Spain, and Departamento de Física Aplicada II, Facultad de Ciencias, Universidad del País Vasco, Apartado 644, E-48080 Bilbao, Spain

Received: January 26, 2007; In Final Form: May 21, 2007

Different kind of measurements were performed on the liquid crystal nonyloxycyanobiphenyl (9OCB) to carry out a study of the molecular dynamics in the smectic A (SmA), nematic (N), and isotropic (I) phases as well as an exhaustive analysis of both the SmA-to-N and N-to-I phase transitions. For the dynamic study, broadband dielectric spectroscopy (10^2 to 1.8×10^9 Hz) was used. Two orientations (parallel and perpendicular) of the molecular director with regard to the probing electric field were investigated. From this study, the static dielectric permittivity was obtained in both alignments and, in addition, the molecular motions that contribute to each one were discussed. The static dielectric data together with specific heat and volumetric determinations were analyzed, proving that both phase transitions are weakly first order, displaying a nearly tricritical behavior. However, the width of metastable regions seems to be dependent on the physical magnitude, although specific heat and volumetric determinations allow for comparable results. It should be noticed that the temperature derivative of the static dielectric permittivity, specific heat, and isobaric thermal expansion coefficient data derived from volumetric determinations are related to each other by scaling relationships.

1. Introduction

The alkyloxycyanobiphenyls *n*OCB (*n* being the number of carbons in the alkyl chain) are liquid crystals very similar to the well-known and exhaustively studied alkylcyanobiphenyls *n*CB. However, whereas the latter were the subject of a great deal of interest during the past nearly 30 years because of their promising technical applications (either as bulk or confined to porous media) and also because they are excellent materials to test the different theoretical proposals about phase transitions, strangely, the studies about the *n*OCBs have been scarce.

Nonyloxycyanobiphenyl (9OCB) is a liquid crystal for which, to the best of our knowledge, very few studies can be found in the scientific literature. If only specific studies on phase transitions and dielectric properties of their mesophases are taken into account, the references are nearly nonexistent.[1,2] However, nonylcyanobiphenyl (9CB), the homologous compound without oxygen in the molecular formula, was and is still now subject of numerous studies, even if the subject matter is only devoted to the study of the mesophase-physical properties and the critical behavior of the phase transitions:[3−17] smecticA(SmA)-to-nematic(N) and N-to-isotropic (I). The phase sequence displayed by 9OCB is exactly the same as its homologous 9CB, being on cooling from the isotropic liquid: N, SmA, and finally Cr (ordered crystalline state). Likewise, although transition temperatures are not the same, both compounds exhibit comparable nematic ranges NR ($= T_{NI} - T_{AN}$; T_{NI} and T_{AN} are the N-to-I and SmA-to-N transition temperatures, respectively) with the same McMillan's ratio,[18] defined as T_{AN}/T_{NI}, of 0.994.[1,5]

According to McMillan,[18] Kobayashi,[19] and de Gennes[20] (the so-called MKG theory), the SmA-to-N transition should be second-order in nature, belonging to the 3D-XY-universality class (specific heat critical exponent $\alpha_{XY} = -0.007$). However, owing to a coupling between nematic and smectic order parameters, strongly influenced by the extension in temperature of the nematic range, a crossover behavior from the strict second-order transition (3D-XY-universality class) up to the tricritical point (TCP ($\alpha_{TCP} = 0.5$), beyond which the SmA-to-N transition becomes first-order in nature, is observed. The stronger the coupling occurs the more McMillan's ratio approaches 1. A value of 0.87 is the theoretical McMillan's limit for the TCP, but experimental data point out values somewhat higher, ranging from 0.942 to 0.994, displaying a nonuniversal value, strongly dependent on the polarity or nonpolarity of the material molecules.[21] As for 9CB and 9OCB, both compounds have nearly identical polar molecules as well as the same McMillan's ratio, and then their critical behavior at the SmA-to-N phase transition should be expected to be similar. However, the great amount of experimental data on 9CB exhibits something puzzling about the character of its SmA-to-N phase transition. Some data allow for a character either tricritical or even first order in nature.[6,7,10,16] Other data exhibit a crossover second-order transition with critical exponents near its tricritical value.[3,8,9,12,22] Even a few years ago, some of the authors of this paper measured the specific heat of 9CB, pure and mixed with other related liquid crystals, obtaining controversial results about the SmA-to-N critical behavior. In addition to these results, Halperin, Lubensky, and Ma[23,24] published a theory, denoted as HLM theory, according to which the SmA-to-N transition should always be weakly first-order in nature. Although HLM theory has not yet been rigorously proved, experimental studies,[6,7,25−27] by means of novelty techniques,

* Author to whom correspondence should be addressed. E-mail: david.orencio.lopez@upc.es.

[†] Laboratori de Caracterització de Materials (LCM), Departament de Física i Enginyeria Nuclear, ETSEIB, Universitat Politècnica de Catalunya.

[‡] Departamento de Física Aplicada II, Facultad de Ciencias, Universidad del País Vasco.

10.1021/jp070689v CCC: $37.00
Published on Web 07/07/2007

were undertaken in the past decade of the 20th century, some of them involving 9CB.[6,7]

The N-to-I phase transition in liquid crystals seems to be one of the most frequently studied transitions both theoretically and experimentally. From the different theoretical approaches, the simplest and maybe the best-known is the mean field given by Landau−de Gennes (L-dG theory)[20] in which an expansion of the free energy density in terms of the nematic-order parameter up to the fourth-order contains a cubic term responsible of the first-order character of the N-to-I phase transition. In such a case, this order−disorder phase transition would not display a critical point if a strong external field is not applied.[25,26] However, the fluidlike model, suggested earlier by Mukherjee,[28,29] proposed the existence of an hypothetical critical region at the first-order transition temperature (T_{NI} is a fluidlike critical temperature) and also on the spinodal curve (T^*_{NI} and T^{**}_{NI} are spinodal temperatures) at which the L-dG theory may break down. Both temperatures, T^*_{NI} and T^{**}_{NI}, are the metastable limits of the I and N phases, respectively. The simple L-dG theory leads to the same effective critical exponents (α_N) and order parameter (β) in the nematic phase, being 0.5, while in the isotropic phase, α_I is set equal zero. These theoretical predictions are noncompatible with experimental results that seem to point out a nearly tricritical behavior in which $\beta = 0.25$ and $\alpha_N = \alpha_I = 0.5$. This tricritical behavior was suggested earlier by Keyes[30] and appears in the mean-field approach assuming a sixth-order expansion in terms of the nematic-order parameter of the free energy density. Although it seems established that experimental data related to this transition can be well described by means of the tricritical hypothesis, some details concerning the characteristic temperatures (T_{NI}, T^*_{NI}, and T^{**}_{NI}) and their relative differences seem to depend on the experimental technique and they still remain a puzzle.[31−34] From a theoretical point of view, volumetric and calorimetric results are compatible with the predictions of the tricritical model, assuming a coupling between the nematic-order parameter and the density.[35] Regarding the experimental data, it seems that volumetric and calorimetric measurements give comparable results, but it remains a certain discrepancy with those reported from dielectric measurements.[34] Strangely, experimental information on the literature devoted to the N-to-I transition of 9CB[5,15,17,36] is scarce and to a much lesser extent if 9OCB is considered.

The purpose of the present paper is to provide the most complete thermodynamic description of both the SmA-to-N and N-to-I phase transitions of 9OCB compound and also to study the dynamics near both phase transitions through dielectric relaxation studies. Among thermodynamic quantities that are able to present singularities at the phase transitions, specific heat at normal pressure as a function of temperature is one of the most widely measured with the required accuracy. If one would like to complete the thermodynamic description, other magnitudes, such as the molar volume or static dielectric permittivity obtained from dielectric relaxation studies, also measured as function of temperature, would be required. Precise molar volume data allow us to get an estimation of the isobaric thermal expansion coefficient (α_p) as a function of temperature in such a way that the critical exponents characterizing their divergences should be the same as those calculated for the specific heat determinations.[32,37,38] In fact, this similarity was first proved by Pippard[39] and later by Garland[40] along the λ transition. Of particular interest in the context of this paper is the scaling relationship on the critical line in which the derivative of the static dielectric permittivity (ϵ_{mean} and ϵ_{iso}) with temperature seems to be proportional to the specific heat as it was earlier predicted by Mistura[41] in 1974 and much more recently evidenced by Rzoska et al.[42] for the N-to-I phase transition of the 7OCB.

The paper is organized as follows. In Section 2, we describe the experimental details. In Section 3, we present and discuss the results: dielectric relaxation and static dielectric studies, specific heat as well as volumetric studies, all of them concerning the SmA, N, and I phases and their transitions. Finally, in Section 4, a summary of the main conclusions is made.

2. Experimental Section

2.1. Materials. The pure component 9OCB was synthesized and purified by Prof. Dabrowsky at the Institute of Chemistry, Military University of Technology, Warsaw, Poland. The purity was stated to be higher than 99.9%, and no further purification was made.

2.2. Specific Heat Measurements. Static specific heat data at constant pressure were obtained through the MDSC technique via a commercial TA Instruments DSC 2920, for which extensive details can be found somewhere else.[1,43−47] It is important to realize that, similar to an ac calorimeter, MDSC technique, besides specific heat data, simultaneously provides phase shift data (δ) that allow determining the coexistence region in weakly first-order transitions. In such a case, the experimental conditions were adjusted in such a way that the phase lag ϕ ($\delta = (\pi/2) - \phi$) between the heat flow rate and temperature rate oscillations was nearly zero out of the phase transition and the imaginary part of the complex specific heat data vanished. Likewise, by means of a special calibration procedure in which very precise latent heat data measured from other homologous compounds through adiabatic calorimetry are considered, MDSC technique is also suitable for quantitative measurements of latent heats of first-order transitions, even if they are weak.

The measurements were performed on cooling from the I phase down to the SmA mesophase and next on heating, both at 0.01 K·min^{-1}, with a modulation temperature amplitude of ±0.035 K and a period of 25 s.

2.3. Dielectric Measurements. Measurements of the complex permittivity $\epsilon^*(\omega) = \epsilon'(\omega) - i\epsilon''(\omega)$, in the range 10^2 to 1.8×10^9 Hz, were performed using two impedance analyzers: HP 4192A and HP 4291A. The cell consists of two gold-plated brass electrodes (diameter 5 mm) separated by silica spacers, making a plane capacitor. A modified HP 16091A coaxial test fixture was used as the sample holder. It was held in a cryostat from Novocontrol, and both temperature and dielectric measurements were computer controlled. Two different alignments of the sample in the plane capacitor were considered: parallel (director parallel to the probing electric field) and perpendicular (director perpendicular to the probing electric field). For the former, no treatment of the electrodes was necessary to get a correct alignment, even without a dc bias voltage. To obtain perpendicular alignment, both metal electrodes were, beforehand, spin-coated with PI2555 polyamide (HD Microsystems) following the procedure described in the manufacturer recipe and next, rubbed uniaxially to obtain the required alignment of the liquid crystal molecules. It is important to realize that the polyamide layers, although they are very thin, contribute to the measured capacity in such a way that a correction procedure was performed. Additional details of such a procedure and also about the technique can be found elsewhere.[46,48,49]

The measurements were performed on heating and on cooling with stabilization at different temperature steps with a temperature control of 20 mK.

2.4. Volume Measurements. Molar volume measurements were obtained through a commercial Anton-Paar DMA-5000 density meter for which a homemade filling device was used. The temperature was controlled with a precision of about ±1 mK. As was investigated by Zywocinski,[50] differences in viscosity between the sample and the standards used for calibration are crucial to obtain high-resolution measurements. Following his recommendation, two homologous liquid-crystal 8OCB (octyloxycyanobiphenyl) and 8CB (octylcyanobiphenyl), for which high-resolution density data provided from dilatometric measurements are available in the literature,[32,38,51] were used as two calibration standards in the investigated temperature range.

The measurements, spanning a temperature range of about 10 K around phase transitions, were performed on heating and on cooling with stabilization at different temperature steps of about 10 mK.

3. Results and Discussion

3.1. Dielectric Relaxation Study. In nematogenic or smectogenic liquid crystals, assuming rigid dipolar molecules, the dielectric relaxation spectra can be analyzed through the general theory developed by Nordio et al.[52] according to which the molecular motions in the frequency domain give rise to four relaxation modes: two of them (ω_1, ω_2) for the parallel permittivity and the other two (ω_3, ω_4) for the perpendicular one. The molecular assignment usually accepted[53] is that ω_1 corresponds to molecular rotations around the short molecular axis; ω_2 is due to molecular rotations around the long molecular axis, ω_3 corresponds to the precessional motion of the molecules around the director, and ω_4 to rotations of the precessing molecules around long axis. One of the major difficulties in such analysis arises when the different relaxation modes occur closely spaced in the frequency domain in such a way that dielectric loss peaks appear partially superimposed. In addition, often the spectral shape of each mode does not correspond to a pure exponential Debye relaxation and the analysis should be performed using the empirical Havriliak−Negami (H−N) function, given as

$$\Delta\epsilon_k(\omega) = \frac{\Delta\epsilon_k}{(1 + (i\omega\tau_k)^{\alpha})^{\beta}} \qquad (1)$$

where $\Delta\epsilon_k$ is the dielectric strength, τ_k the relaxation time, k the number of the relaxation process, and α,β parameters describing the shape (symmetry and width), $\alpha = \beta = 1$ corresponds to Debye relaxation.

Figure 1 shows two three-dimensional plots of the imaginary part of the dielectric permittivity vs temperature and frequency of 9OCB for the SmA, N, and I phases in which two molecular alignments have been considered. In part A, both the SmA and N mesophases are in parallel alignment, whereas in part B, both mesophases are in perpendicular alignment. At first glance, in Figure 1A, the dielectric spectra seem to be dominated by the ω_1 mode, whatever phase is considered (I, N, or SmA). However, in Figure 1B, although in the I phase the spectra seem to be also dominated by the same ω_1 mode, when the I-to-N phase transition takes place, a deep decrease of the dielectric response occurs and the losses appear as a very broad peak.

Let us analyze in detail these results. Figure 2A shows both components (real and imaginary parts) of the dielectric permittivity in the I phase at 357 K. The results were fitted to two near-Debye modes ($\alpha = 1$ for the high-frequency mode and $\alpha = 0.93$ for the low-frequency one). The high-frequency mode

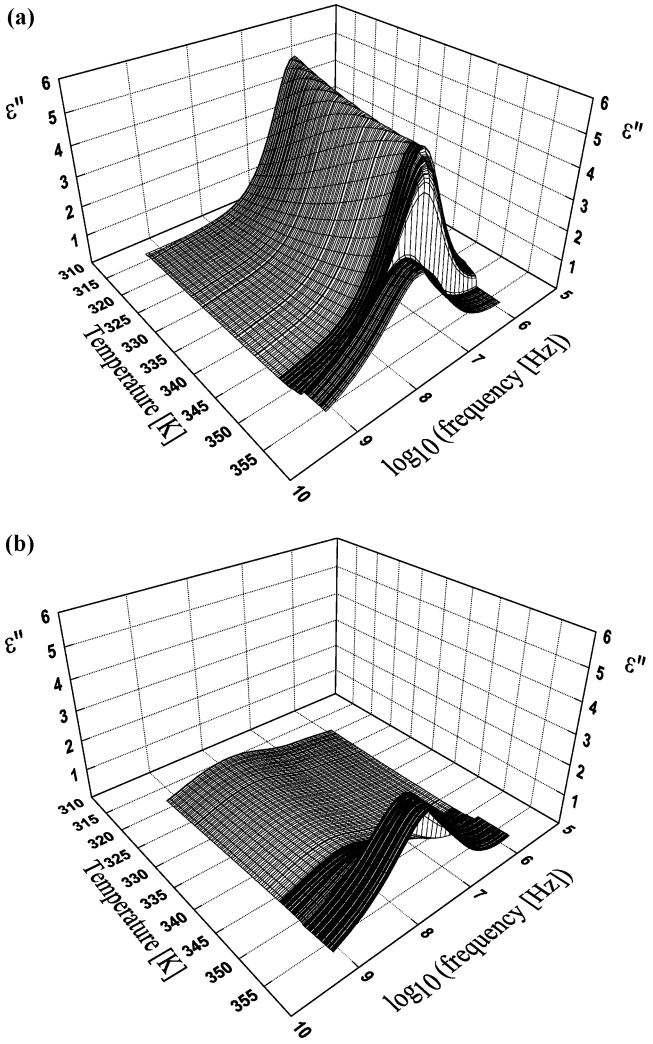

Figure 1. Three-dimensional plots of dielectric losses vs temperature and frequency for 9OCB in parallel (A) and perpendicular (B) alignments.

could be attributed to the rotation around the long molecular axis (ω_2 mode), whereas the low-frequency one is assigned to molecular rotations around the short molecular axis (ω_1 mode). This mode ω_1 is dominant in the relaxation spectra because the dipole moment (due to the CN and CO polar groups, which do not have the same direction[54]) is, even so, nearly aligned along the long molecular axis. Our fittings of the relative strength data of both modes in the I phase, $\Delta\epsilon_1 \propto \mu_l^2$ and $\Delta\epsilon_2 \propto \mu_t^2$, have allowed to estimate the angle between the dipole moment and the long molecular axis as about 19°. Although no data in the literature about this angle have been found, its results are comparable to the values obtained for other *n*OCB compounds.[47] It should be noted that many authors fit the dielectric data of *n*CB and *n*OCB compounds in the I phase to only one broad relaxation.[55−57] This is also possible with our data, the fittings to only one mode being Cole−Davidson ($\beta = 0.65$). Our choice of two modes in the I phase arises from the fact that, in both mesophases, either N or SmA, in parallel alignment, the fitting to only one mode is extremely deficient. So, to overcome this inconvenience, two modes must be considered in the mesophases (SmA or N), and so they should be also considered in the I phase whenever the rotational diffusion tensor were anisotropic.[58−60]

Figure 2B shows both components (real and imaginary parts) of the dielectric permittivity (parallel alignment) in the N phase at 352 K. Although the dielectric permittivity is not shown in

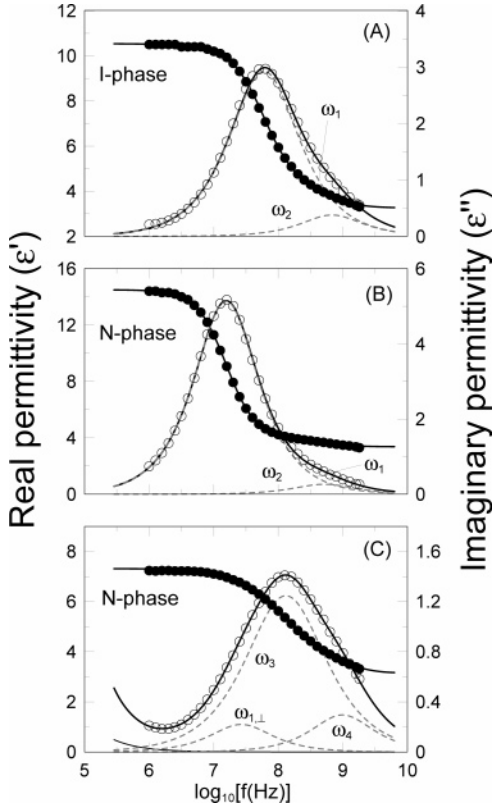

Figure 2. Frequency dependence of the dielectric permittivity of 9OCB in the isotropic phase ($T = 357$ K) (A) and in the nematic phase ($T = 352$ K) in both the parallel (B) and perpendicular (C) alignments. Thick black solid lines are fittings according to eq 1. Dashed lines represent deconvolution into elementary modes.

the SmA mesophase with the sample in parallel alignment, we can anticipate that no qualitative differences are observed with the values shown in this figure. Our analysis reveals a situation comparable to that which is shown in Figure 2A in the I phase: two adjacent processes identified as ω_1 mode (the most prominent at lower frequencies being near-Debye at $\alpha = 0.97$, $\beta = 1$) and ω_2 mode (at higher frequencies being also near Debye with both fixed $\alpha = 1$, $\beta = 1$).

Figure 2C shows both components (real and imaginary parts) of the dielectric permittivity in the N mesophase (with the sample in perpendicular alignment) at 352 K. In perfect perpendicular alignment, only two processes associated to the precessional motion of the long axis around the director (ω_3 mode) and the rotation around the long axis of the precessing molecule (ω_4 mode) should be considered. However, to fit our data, a third mode in the low-frequency side is required. This mode, denoted as $\omega_{1\perp}$, is related to the molecular rotations around the short axis and has been evidenced prior to this study for other homologous compounds.[48,49] It is a consequence of a nonperfect perpendicular alignment, a fact that nearly always happens because the axis of magnetic or dielectric maximum susceptibility does not coincide with the steric main axis. The same idea is applicable when the director is forced by surface effects that align the molecules. So, from Figure 2C, the most prominent relaxation at an intermediate frequency is associated to mode ω_3 ($\alpha = 0.87$, $\beta = 1$), whereas the higher-frequency process corresponds to mode ω_4 and the lower-frequency process to the mode $\omega_{1\perp}$, both Debye-like. Again, the results in the SmA mesophase are similar to what is found in the N phase.

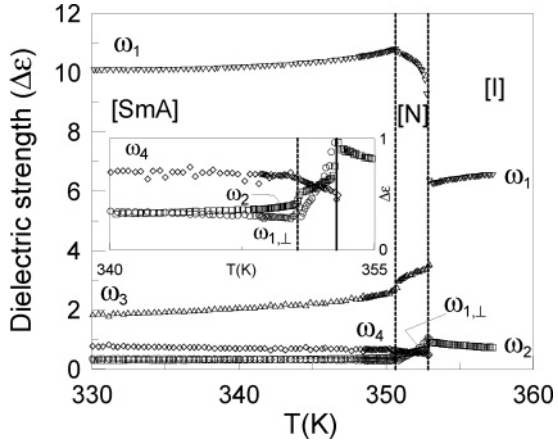

Figure 3. Dielectric strength data as a function of temperature of the different elementary contributions for 9OCB. The assigned symbols are the following: down triangles (ω_1 mode), squares (ω_2 mode), up triangles (ω_3 mode), diamonds (ω_4 mode), and circles ($\omega_{1\perp}$ mode). The inset shows a zoom for $\omega_{1\perp}$, ω_2, and ω_4 modes.

Although in Figure 2 the spectra in the 10^6 to 1.8×10^9 Hz frequency range only have been shown, measurements down to 10^2 Hz were also performed. These measurements did not reveal the existence of any additional process.

Figure 3 shows the temperature dependence of the dielectric strength for all the aforementioned modes. The behavior is as expected from the Maier and Meier equations[61] on going from the I to the N phase (parallel alignment). The dielectric strength of mode ω_1 increases at the I-to-N phase transition due to the onset of the nematic order and inside the N-mesophase increases as temperature decreases, i.e., as the orientational order increases. However, in the SmA mesophase, the strength data tend to diminish from the SmA-to-N transition down to lower temperatures. This fact could be related to an increase of the antiparallel correlation. At low enough temperatures, an effect of the saturation in the strength data is clearly visible not only in the data associated to this mode but also in those corresponding to the other relaxation modes. This behavior is expected to be common for other smectogenic-like compounds.[49] The dielectric strength of mode ω_2 (parallel alignment) in both mesophases, either N or SmA, behave as expected; it decreases as temperature decreases, i.e., as the orientational order increases. The dielectric strength (perpendicular alignment) in the N mesophase of mode ω_3 decreases, but that of ω_4 mode increases, as predicted by the Maier and Meier equations.[61] The dielectric strength of $\omega_{1\perp}$ mode (perpendicular alignment) with temperature in the N mesophase, which is due to a nonperfect perpendicular alignment, abruptly decreases as temperature does (inset of Figure 3), very close to the N-to-I transition, giving rise to very small values in the SmA mesophase.

Figure 4 shows, in an Arrhenius plot, the temperature dependence of the characteristic relaxation frequency data associated to each mode for the different phases (SmA, N, and I). It is clearly observed in Figure 4 and in more detail in Figure 5 that the characteristic frequency of ω_1 mode (f_1) exhibits a jump to lower frequencies at the I-to-N transition and a much less pronounced jump at the N-to-SmA transition when the sample is in parallel alignment. To investigate properly the Arrhenius behavior of f_1, the methodology proposed by Jadzyn et al.[17,62] is followed. In such a methodology, the Arrhenius law ($f_1 = f_0 e^{-E_A/RT}$) in which E_A is the activation energy, R is the gas constant, and f_0 is a pre-exponential factor should be

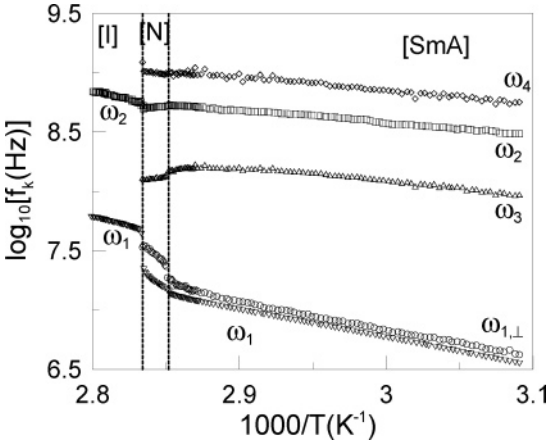

Figure 4. Arrhenius plot of the relaxation frequencies (f_k) of the different elementary contributions for 9OCB. The assigned symbols are the following: down triangles (ω_1 mode), squares (ω_2 mode), up triangles (ω_3 mode), diamonds (ω_4 mode), and circles ($\omega_{1\perp}$ mode). The inset shows a zoom for $\omega_{1\perp}$, ω_2, and ω_4 modes.

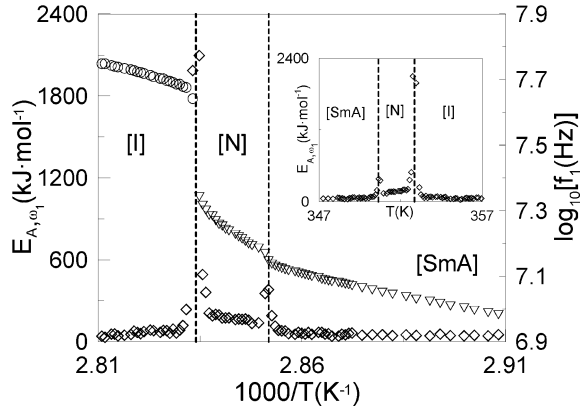

Figure 5. Arrhenius plot of the relaxation frequency (open circles and open-down triangles) (right *y*-axis) and the instantaneous activation energy (open diamonds) (left *y*-axis), both corresponding to ω_1 mode. The inset shows the instantaneous activation energy corresponding to ω_1 mode vs temperature.

recalled. The differentiation of $\log(f_1)$ over T^{-1} through the Arrhenius law leads to the activation energy associated to ω_1 mode ($E_{A,\omega 1}$) at each temperature. This has been made by distortion-sensitive derivative analysis of the experimental data from Figure 4, and the resulting $E_{A,\omega 1}$ are presented in Figure 5. From this figure, it seems that the Arrhenius behavior is satisfied in the I, N, and SmA phases, with the exception made of phase transitions and excluding regions (about 0.5 K apart). However, unlike its homologous 9CB,[17] no strong deviations from Arrhenius law in the whole N phase due to both phase transitions are observed, as seen in Figure 5 and in the inset. There is another interesting fact to be remarked concerning the activation energies for each phase. As it can be easily observed, both I and SmA phases have comparable activation energies of about 60 kJ·mol^{-1}, while N mesophase displays values about 170 kJ·mol^{-1}. So, it seems that the energy barrier hindering the molecular motions around the short molecular axis is comparable in both I and SmA phases and smaller than that found in the N phase.[63] These activation energy values are comparable to those obtained for other smectogenic-like compounds[49] for which the N range is broader in temperature.

As for the characteristic frequency of ω_2 mode (f_2), as can be seen in Figure 4, the changes at the phase transitions are very smooth. Although it seems that the activation energy in the I phase is comparable to that of ω_1 mode, in the SmA phase,

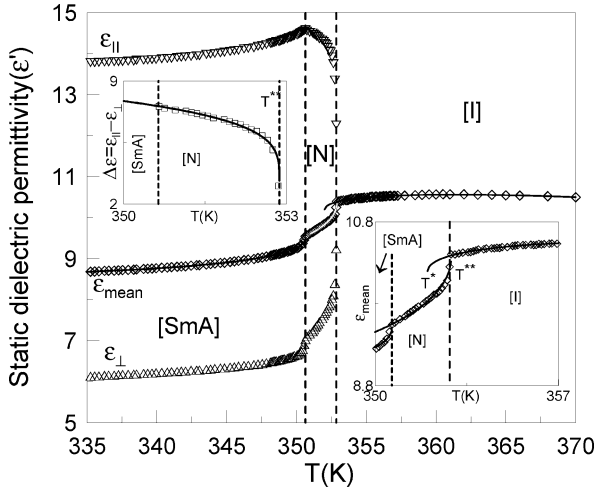

Figure 6. Static dielectric permittivity behavior in the I, N, and SmA phases of 9OCB. The right-bottom inset shows the behavior of the mean dielectric permittivity in the N mesophase and the dielectric permittivity in the I phase through the N-to-I phase transition. Grey solid lines are fittings using eqs 2a and 2b. The left-top inset shows the dielectric anisotropy in the N mesophase vs temperature. Black solid line corresponds to a fitting according to eq 3.

it (parallel alignment) is smaller (about 10 kJ·mol^{-1}) as expected. Anyway, it is important to realize that the fittings according to eq 1 of this high-frequency mode are very difficult to obtain near-phase transitions because of its low dielectric strength (see Figure 3).

As for the characteristic frequencies relating the modes ω_3, ω_4, and $\omega_{1\perp}$, all of them appearing in the mesophases with the sample in perpendicular alignment, two observations can be made from Figure 4. The first one related to the $\omega_{1\perp}$ mode, which displays comparable activation energies to those found for the ω_1 mode (parallel alignment), but the jump at the N-to-SmA transition seems more pronounced to what is found for the latter, likely due to the difficulty in performing the fittings according to eq 1. The second observation arises from the characteristic frequency of the ω_3 mode, which slightly increases in the N phase and slowly decreases in the SmA phase with a comparable activation energy to that found for the ω_2 mode. This fact could be due to the increasing of the orientational order parameter and at lower temperatures to viscosity effects.

3.2. Static Dielectric Permittivity Study. The temperature dependence of the static dielectric permittivity for parallel and perpendicular alignments is shown in Figure 6. These quantities have been calculated by adding the dielectric strengths plus the high-frequency limit, ϵ_∞, as deduced from the fittings of the complex dielectric permittivity. Additional data at high temperatures in the I phase have also been considered from static measurements at 10^5 Hz and have been included in Figure 6. The parallel component ($\epsilon_{||}$) and the permittivity in the I phase (ϵ_{iso}) have been easily obtained from the strength data corresponding to ω_1 and ω_2 modes and the corresponding ϵ_∞ for these relaxations. It may be underlined that both the isotropic permittivity and the parallel component basically involve molecular rotations around the short axis (the main contribution is due to ω_1 mode). Likewise, in both SmA-to-N and N-to-I phase transitions, the parallel component mimics the ω_1 strength data. The perpendicular component ($\epsilon_\perp$) arises from the strength data corresponding to ω_3, ω_4, and $\omega_{1\perp}$ modes and the corresponding ϵ_∞ for these relaxations. The main contribution to the perpendicular component comes from the precessional motion of the long axis around the director (ω_3 mode), and it may be said that this component is nearly unaffected in the SmA

TABLE 1: Phase Transition Temperatures, Metastable Difference Temperatures (ΔT^{**}, ΔT^{*}), the Width of the Metastable Region ($T^{**} - T^{*}$) ,and the Ratio ($\Delta T^{*}/\Delta T^{**}$)

phase transition	T (K)	ΔT^{**} (K)	ΔT^{*} (K)	$(T^{**} - T^{*})$ (K)	$\Delta T^{*}/\Delta T^{**}$	physical magnitude
SmA−N	350.64	0.03	0.58	0.61	19 ± 14	dielectric constant[a]
	351.08[b]	0.02	0.05	0.05	3 ± 2	specific heat
	351.01	0.02	0.08	0.10	4 ± 3	molar volume
N−I	352.85	0.06	0.85	0.91	14 ± 6	dielectric constant
		0.02				order parameter
	353.22[b]	0.14	0.29	0.43	2 ± 1	specific heat
	353.16	0.07	0.39	0.46	6 ± 2	molar volume

[a] Fittings according to equations such as eq 6. [b] Data already published in ref 1 in which a brief summary of the available thermal information from different bibliographic sources was made.

TABLE 2: Results of the Fittings for the N−I Phase Transition of 9OCB

dielectric constant (ϵ_{mean}; ϵ_{iso}) fitting to eq 2		specific heat (C_p) fitting to eq 4		molar volume ($\ln v$) fitting to eq 6	
ϵ^{**}	10.367 ± 0.009	B_C ($J{\cdot}K^{-1}{\cdot}g^{-1}$)	2.185 ± 0.005	$E^{v}_{0,N}$	5.795 ± 0.001
ϵ^{*}	10.192 ± 0.006	D_C ($J{\cdot}K^{-1}{\cdot}g^{-1}$)	-22 ± 2.0	$E^{v}_{0,I}$	5.796 ± 0.001
a_N (K^{-1})	0.056 ± 0.007	$A_{C,N}/A_{C,I}$	2.9 ± 0.9	$10^5 \times E^{v}_1$ (K^{-1})	112 ± 29
a_I (K^{-1})	-0.040 ± 0.001	T^{**} (K)	353.36 ± 0.01	$10^5 \times E^{v}_{2,N}$ (K^{-2})	-11 ± 3
$A_{\epsilon,N}/A_{\epsilon,I}$	-2.5 ± 0.2	T^{*} (K)	352.93 ± 0.09	$10^5 \times E^{v}_{2,I}$ (K^{-2})	-16 ± 5
T^{**} (K)	352.91 ± 0.04	α_N	0.50 ± 0.05	$A_{v,N}/A_{v,I}$	-2.3 ± 0.9
T^{*} (K)	352.00 ± 0.01	α_I	0.50 ± 0.05	T^{**} (K)	353.23 ± 0.04
α_N	0.52 ± 0.03	$10^3 \times \chi^2_N$	3	T^{*} (K)	352.77 ± 0.02
α_I	0.50 ± 0.01	$10^3 \times \chi^2_I$	2	α_N	0.50 ± 0.01
$10^4 \times \chi^2_N$	4			α_I	0.50 ± 0.03
$10^5 \times \chi^2_I$	3			$10^{10} \times \chi^2_N$	2
				$10^{10} \times \chi^2_I$	2.5

mesophase due to the other contributions (ω_4 and $\omega_{1\perp}$ strength data). However, the situation close to the N-to-I transition temperature and even in the narrow N range is clearly different. In fact, it could even be said that the evolution of $\epsilon_\perp$ in the N range is hardly affected by residual molecular rotations around the short axis ($\omega_{1\perp}$ mode). The mean dielectric permittivity $\epsilon_{mean} = {}^1/_3(\epsilon_{||} + 2\epsilon_\perp)$ is also shown in Figure 6 and in a zoom window around the N-to-I transition in the inset at the right-bottom of this figure.

Let us now consider both phase transitions in a most quantitative way. In Table 1, in addition to other quantities to be commented later, transition temperatures obtained from dielectric permittivity along with those obtained from other physical magnitudes are consigned, being the dielectric NR (nematic range) of 2.21 K. To analyze dielectric data at the N-to-I phase transition, it is often used the following equations:[42,47,62]

$$\epsilon_{iso} = \epsilon_H = \epsilon^{*} + a_H|T - T^{*}| + A_{\epsilon,H}|T - T^{*}|^{1-\alpha} \quad \text{for } T > T_{NI} = T^{*} + \Delta T^{*} \quad (2a)$$

$$\epsilon_{mean} = \epsilon_L = \epsilon^{**} + a_L|T - T^{**}| + A_{\epsilon,L}|T - T^{**}|^{1-\alpha} \quad \text{for } T < T_{NI} = T^{**} - \Delta T^{**} \quad (2b)$$

where T^{**} denotes the temperature at which the N-to-I transition would occur coming from the N phase if it were second-order and T^{*} has the same meaning when temperature decreases from the I phase. The permittivity above the transition (in this case, I phase) and below (in this case, N phase) is denoted as ϵ_H and ϵ_L, respectively. The extrapolated value of the ϵ_{iso} at T^{*} is ϵ^{*} and the ϵ_{mean} at T^{**} is ϵ^{**}. α is the specific heat critical exponent (α should be about 0.5 according to the tricritical hypothesis). The other parameters (a_H, $A_{\epsilon,H}$, a_L, $A_{\epsilon,L}$) along with those cited above must be obtained by fitting the corresponding dielectric data. Both ΔT^{*} and ΔT^{**} or, even better, the difference ($T^{**} - T^{*}$) represent the width of the metastable region at the N-to-I phase transition and, along with other thermodynamic properties such as the latent heat (ΔH) and volume jump (Δv), may give an indication of how first-order the transition is. In Table 2, the fitted parameters in the N and I phases according to eqs 2a and 2b are consigned. All these parameters represent well enough the measured permittivity data as indicated by χ^2 values and as can be seen in Figure 6 as well as in more detail in the right-bottom inset in which both equations are drawn. Although the static permittivity displays a maximum in the I phase as its homologous 9CB,[17] it seems less pronounced and is located at higher temperatures. Consequently, the fitted T^{*} is closer to the nematic clearing temperature (T_{NI}), being ΔT^{*} even lower than 1 K (see Table 1). The same parameter in 9CB is slightly higher than 3 K obtained from dielectric data as well.[17] It is important to realize that the fittings related to the N phase are handicapped by the narrow N range. Even so, the α exponent seems to be near 0.5 (in the error band) and the χ^2 value is acceptable (see Table 2).

Another approach to test the N-to-I transition in the N side arises from the evolution with temperature of the nematic order parameter. Taking into account the dielectric anisotropy ($\Delta\epsilon = \epsilon_{||} - \epsilon_\perp$) in the N phase, $\Delta\epsilon$ is proportional to the nematic order parameter in such a way that:[42,47]

$$\Delta\epsilon = \Delta\epsilon^{**} + B|T - T^{**}|^{\beta} \quad (3)$$

where T^{**} has the same meaning as in eq 2b and β is the critical exponent associated to the order parameter, which should be 0.25 according to the tricritical hypothesis. In the inset at the left-top of Figure 6, $\Delta\epsilon$ against temperature is shown along with the fitting through eq 3. The most relevant parameters in such an equation, are T^{**} and β, which are found to be 352.87($\pm$0.02) K and 0.25($\pm$0.02), respectively. Both ΔT^{**} values calculated from T^{**} through eqs 2b or 3 are comparable (see Table 1).

The analysis of the SmA-to-N phase transition from dielectric data is nonevident. At first glance, although no references in the literature have been found, it could also be tried by assuming

TABLE 3: Results of the Fittings for the SmA-to-N Phase Transition of 9OCB

dielectric constant (ϵ_{mean})				specific heat (C_p)		molar volume ($\ln v$)	
fitting to eq 2		fitting to equations such as eq 6[a]		fitting to eq 4		fitting to eq 6	
ϵ^**	9.52 ± 0.01	$E^{\epsilon}_{0,S}$	9.533 ± 0.003	B_C ($J \cdot K^{-1} \cdot g^{-1}$)	2.44 ± 0.07	$E^{v}_{0,S}$	5.790 ± 0.001
ϵ^*	9.4 ± 0.1	$E^{\epsilon}_{0,N}$	9.2 ± 0.1	D_C ($J \cdot K^{-1} \cdot g^{-1}$)	51 ± 2	$E^{v}_{0,N}$	5.790 ± 0.001
a_S (K^{-1})	0.023 ± 0.001	$10^3 \times E^{\epsilon}_1(K^{-1})$	12 ± 2	$A_{C,S}/A_{C,N}$	0.64 ± 0.04	$10^5 \times E^{v}_1(K^{-1})$	96 ± 4
$a_N(K^{-1})$	0.2 ± 0.1	$10^3 \times E^{\epsilon}_{2,S}(K^{-2})$	11 ± 1	T^{**} (K)	351.082 ± 0.010	$10^5 \times E^{v}_{2,S}(K^{-2})$	11 ± 2
$A_{\epsilon,S}/A_{\epsilon,N}$	-26 ± 5	$10^3 \times E^{\epsilon}_{2,N}(K^{-2})$	11 ± 4	T^* (K)	351.03 ± 0.02	$10^5 \times E^{v}_{2,N}(K^{-2})$	11 ± 1
T^{**} (K)	350.6 ± 0.1	$A_{\epsilon,S}/A_{\epsilon,N}$	-0.7 ± 0.1	α_S	0.52 ± 0.03	$A_{v,S}/A_{v,N}$	-0.9 ± 0.1
T^* (K)	350.2 ± 0.9	T^{**} (K)	350.67 ± 0.02	α_N	0.51 ± 0.03	T^{**} (K)	351.03 ± 0.02
α_S	0.53 ± 0.03	T^* (K)	350.06 ± 0.01	$10^3 \times \chi^2_S$	2	T^* (K)	350.93 ± 0.01
α_N	0.53[b]	α_S	0.52 ± 0.02	$10^3 \times \chi^2_N$	3	α_S	0.51 ± 0.05
$10^3 \times \chi^2_S$	0.5	α_N	0.5 ± 0.1			α_N	0.51 ± 0.03
$10^3 \times \chi^2_N$	2	$10^4 \times \chi^2_S$	2			$10^{10} \times \chi^2_S$	4
		$10^3 \times \chi^2_N$	2			$10^{10} \times \chi^2_N$	1

[a] $\epsilon_S = E^{\epsilon}_{0,S} + E^{\epsilon}_1 [T - T^{**}] + E^{\epsilon}_{2,S}[T - T^{**}]^2 + A_{\epsilon,S}|T - T^{**}|^{1-\alpha}$. $\epsilon_N = E^{\epsilon}_{0,N} + E^{\epsilon}_1[T - T^*] + E^{\epsilon}_{2,N}[T - T^*]^2 + A_{\epsilon,N}|T - T^*|^{1-\alpha}$. [b] This parameter has been held fixed.

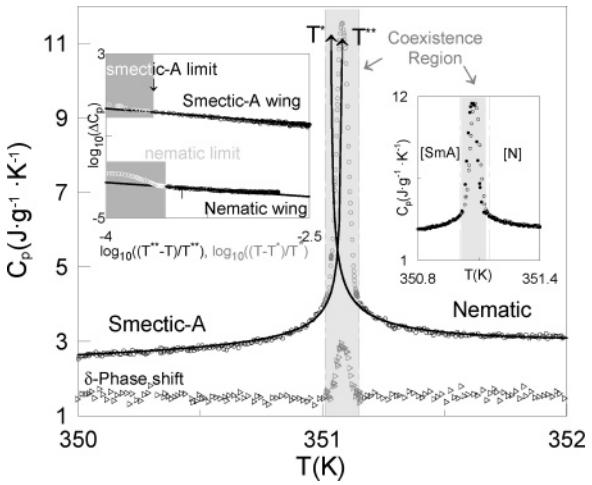

Figure 7. Specific heat (open circles) as a function of temperature near the SmA-to-N transition for 9OCB. δ phase shift data (open-right triangle) are only included to delimit the specific heat coexistence region (shaded area). The left inset shows in a double logarithmic plot ΔC_p-($C_p - C_{p,background}$) vs reduced temperatures. For the SmA wing, $C_{p,background} = B_C + D_C[(T/T^{**}) - 1]$, and for the N wing, $C_{p,background} = B_C + D_C[(T/T^*) - 1]$, ($B_C$ and D_C are taken from Table 3). The right inset shows the hysteresis at the transition.

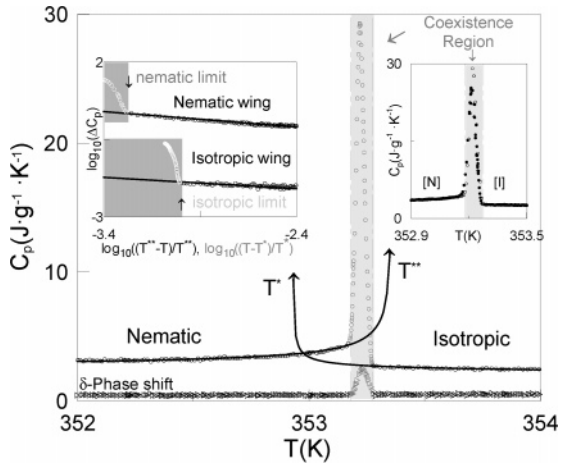

Figure 8. Specific heat (open circles) as a function of temperature near the N-to-I transition for 9OCB. δ phase shift data (open-right triangle) are only included to delimit the specific heat coexistence region (shaded area). The left inset shows in a double logarithmic plot ΔC_p-($C_p - C_{p,background}$) vs reduced temperatures. For the N wing, $C_{p,background} = B_C + D_C[(T/T^{**}) - 1]$, and for the N wing, $C_{p,background} = B_C + D_C$-$[(T/T^*) - 1]$ (B_C and D_C are taken from Table 2). The right inset shows the hysteresis at the transition.

two equations similar to eq 2b, one for the SmA mesophase and another for the N one in which we can define T^* and T^{**} for the N side and SmA side, respectively, with the same meaning as in eqs 2a and 2b. Obviously, if the transition were second-order, both temperatures should coincide. The results of the fittings considering this methodology seem to be unsuccessful (see Table 3 and Figure 6). Although the SmA side seems to provide reasonable fitted parameters, for the N side it is impossible to obtain the critical exponent with a reasonable T^*. If the critical exponent is held fixed to 0.53 (the same as in the SmA side), a reasonable T^* of 350.2 K could be obtained but with an abnormal a_N parameter. Let us revise later the analysis of this transition.

3.3. Specific Heat Study. Specific heat data around both SmA-to-N and N-to-I phase transitions were published a few years ago as a previous study on 9OCB[1] undertaken by some authors of the present paper. As previously cited, the SmA-to N phase transition displays an imperceptible thermal hysteresis, as can be observed in the right-inset of Figure 7, by a very small downward shift at the peak temperature. However, specific heat data on heating and on cooling out of the specific heat coexistence region are identical. The same observation can be done about the N-to-I phase transition, as seen in the right-inset of Figure 8. Obviously, it should be stressed that, if thermal hysteresis is absent, no conclusion about the order of the transition could be done. The existence of thermal hysteresis in both phase transitions, along with sharp peaks in the phase shift (δ), are signatures of their first-order character. In a more quantitative way, a detailed analysis of the specific heat critical behavior at both phase transitions is lacking.

The specific heat data could be well analyzed using the standard expressions[31,47,64] in a region of no more than $\pm$ 3 K around both SmA-to-N and N-to-I transitions but excluding all the points in the coexistence regions

$$C_{p,L} = B_C + D_C\left[\frac{T}{T^{**}} - 1\right] + A_{C,L}\left|\frac{T}{T^{**}} - 1\right|^{-\alpha} \quad (4a)$$

$$C_{p,H} = B_C + D_C\left[\frac{T}{T^{*}} - 1\right] + A_{C,H}\left|\frac{T}{T^{*}} - 1\right|^{-\alpha} \quad (4b)$$

where α, T^*, and T^{**} have the same meaning as in eq 2. The specific heat above and below the transition are denoted as $C_{p,H}$

and $C_{p,L}$, respectively. The $A_{C,L}$ and $A_{C,H}$ are the corresponding amplitudes below and above, respectively, whereas B_C and D_C account for the specific heat background, both being above and below the transition.

Figures 7 and 8 show the specific heat along with δ phase shift data in a region of about ±1 K around both the SmA-to-N and N-to-I phase transitions. δ phase shift data have been used in both figures to identify, by a sharp change, the excluded points of both coexistence regions (shaded area in Figures 7 and 8 and in their insets). As for the SmA-to-N phase transition, a range of data spanning about 1 K has been chosen in both the SmA and N mesophases out of the coexistence region for which eqs 4a and 4b have been used to fit the SmA and N sides, respectively. Common parameters in both phases (B_C, D_C, and α) have been simultaneously refined after a previous independent fitting. As for the N-to-I phase transition, the fitting procedure has been identical to that described for the SmA-to-N phase transition.

All the parameters are collected in Tables 2 and 3 and represent well enough the measured specific heat data around both phase transitions, as indicated by χ^2 values and as seen in Figures 7 and 8, where both eqs 4 are drawn. In the left-insets of both figures, in a double logarithmic plot, a linear relationship, with slope -α, is found for both phase transitions between ΔC_p ($C_p - C_{p,\text{background}}$; $C_{p,\text{background}}$ is calculated from eq 4 using B_C and D_C parameters (Table 2 or 3) and the corresponding reduced temperatures ($(T^{**} - T)/T^{**}$ *or* $(T - T^*)/T^*$) Table 2 or 3).

From Tables 2 and 3, it can be observed that the α-critical exponent is about 0.5 in both phase transitions, the value predicted by the extended L-dG theory or by the tricritical hypothesis. As for the N-to-I phase transition, T^* and T^{**} temperatures along with the specific heat T_{NI} allow us to determine both ΔT^*, ΔT^{**} as well as ($T^{**} - T^*$) as consigned in Table 1. It should be remarked that the uncertainty in the determination of T^* is considerable, as can be seen in Figure 8. The ratio of amplitudes ($A_{C,N}/A_{C,I}$) is about 3, a value very close to those reported for other liquid-crystal-like materials at the N-to-I phase transition[47,64,65] but far from the amplitude ratio for the tricritical behavior of $^3He + {}^4He$, which is found to be about 7.[66] The measured latent heat[1] (ΔH) is about 0.84 kJ·mol^{-1}, a value comparable to that reported by other authors.[2]

Concerning the SmA-to-N phase transition, both T^* and T^{**} temperatures are very close to the specific heat transition temperature (T_{SN}) leading to ΔT^*, ΔT^{**}, and ($T^{**} - T^*$) values much smaller (see Table 1) than those reported for the N-to-I phase transition. The ratio of amplitudes ($A_{C,S}/A_{C,N}$) is about 0.6, a value that is about one-half of that found for the tricritical amplitude ratios of other liquid-crystal-like compounds in the SmA-to-N phase transition[1,43] for which a negligible latent heat was reported. The SmA-to-N latent heat[1] (ΔH) is found to be about 0.16 kJ·mol^{-1}, a value which is about one-half of that reported by Oweimreen et al.[2]

3.3. Volumetric Study and Scaling Relationships. Figure 9 shows the results of the volumetric measurements as a function of temperature in a heating run in a region of about 10 K where both the SmA-to-N and N-to-I phase transitions are present. In both insets, heating and cooling runs around both phase transitions are shown in a zoom window. The thermal hysteresis is clearly visible for the N-to-I phase transition and more subtly for the SmA-to-N. From both insets, volume jumps associated to the SmA-to-N (Δv_{SN}) and to the N-to-I (Δv_{NI}) phase

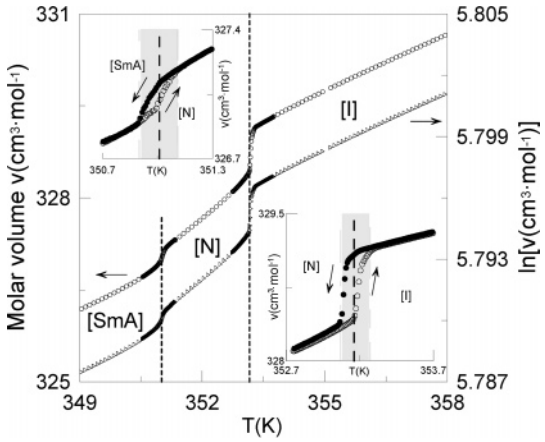

Figure 9. Molar volume (open circles) (left *y*-axis) and the logarithm of the molar volume (open-right triangle) (right *y*-axis) as a function of temperature for 9OCB. The left-top inset shows a zoom window of the molar volume near the SmA-to-N transition. The right-bottom inset shows a zoom window of the molar volume near the N-to-I transition. Open and filled symbols correspond to heating and cooling runs, respectively. Shaded areas represent the molar volume coexistence region.

transitions can be determined as about 0.10 cm^3·mol^{-1} and 0.705 cm^3·mol^{-1}, respectively. The goodness of these values can be evaluated through Clapeyron equation applied to both phase transitions

$$\left(\frac{dp}{dT}\right)_{SN} = \frac{\Delta H_{SN}}{T_{SN}\Delta v_{SN}} \tag{5a}$$

$$\left(\frac{dp}{dT}\right)_{NI} = \frac{\Delta H_{NI}}{T_{NI}\Delta v_{NI}} \tag{5b}$$

where $(dp/dT)_{SN}$ and $(dp/dT)_{NI}$ are the slopes of both phase transitions in a $p-T$ diagram, which are known to be from pressure measurements[67] as about 4.19×10^6 Pa·K^{-1} and 3.24×10^6 Pa·K^{-1}, respectively, at atmospheric pressure. Combining for both phase transitions, data of latent heats (ΔH_{SN} and ΔH_{NI}) and transition temperatures obtained from specific heat measurements with those of volume jumps determined above, eq 5 leads to calculated slopes of about 4.56×10^6 Pa·K^{-1} and 3.37×10^6 Pa·K^{-1} for SmA-to-N and N-to-I phase transitions, respectively.

Figure 9 also shows the logarithm of the molar volume in a heating run. These data in a logarithmic form, both on heating and on cooling experiments, through the distortion-sensitive derivative analysis are allowed to calculate the isobaric thermal expansion coefficient $\alpha_p (= [(\partial \ln v)/\partial T]_p)$ at each temperature. These results are presented in Figure 10A,B along with specific heat data, as an eye-guide, in a region of ±1 K around both the SmA-to-N and N-to-I phase transitions.

As for the α_p data around the SmA-to-N phase transition out of the specific heat coexistence region (shaded area), it is evident that a nearly perfect scaling with those of specific heat data is observed, and so a comparable critical behavior, assuming similar equations to eqs 4a and 4b, with the same critical exponent of about 0.5 and comparable ΔT^*, ΔT^{**}, ($T^{**} - T^*_N$) and the amplitude ratio ($A_{\alpha p,S}/A_{\alpha p,N}$), would be expected. Even so, α_p data display some scattered values inherent to the derivative procedure, which could produce a certain distortion in a fine numerical analysis of data. This inconvenience could

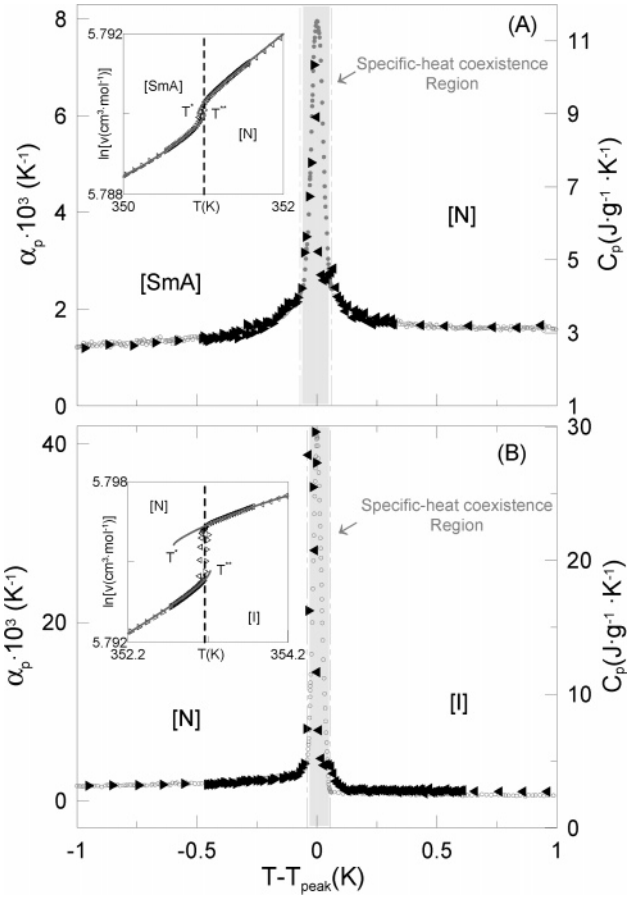

Figure 10. Calculated thermal expansion coefficient data (black-filled symbols) and specific heat data (gray open symbols) near the SmA-to-N transition (A) and near the N-to-I transition (B) as a function of ($T - T_{peak}$) for 9OCB. Both insets show the logarithm of the molar volume vs temperature along with the fittings according to eqs 6a and 6b (gray solid lines).

be overcome by analyzing original data, as for example ln υ, through integrated equations of the same type as eq 4, assuming validity in a region of no more than ±3 K around phase transitions:

$$\ln \upsilon_{\mathrm{L}} = E^{\upsilon}_{0,\mathrm{L}} + E^{\upsilon}_{1}[T - T^{**}] + E^{\upsilon}_{2,\mathrm{L}}[T - T^{**}]^2 + A_{\upsilon,\mathrm{L}}|T - T^{**}|^{1-\alpha} \quad (6a)$$

$$\ln \upsilon_{\mathrm{H}} = E^{\upsilon}_{0,\mathrm{H}} + E^{\upsilon}_{1}[T - T^{*}] + E^{\upsilon}_{2,\mathrm{H}}[T - T^{*}]^2 + A_{\upsilon,\mathrm{H}}|T - T^{*}|^{1-\alpha} \quad (6b)$$

where α, T^*, and T^{**} have the same meaning as in eqs 2 and 4. The independent terms $E^{\upsilon}_{0,\mathrm{L}}$ and $E^{\upsilon}_{0,\mathrm{H}}$, different above and below the transition, do not exist in equations to parametrize α_p data (or C_p data). The terms E^{υ}_{1} can be identified with $B_{\alpha p}$ (the parallel to B_C in eq 4), the same above and below the transition. Both $E^{\upsilon}_{2,\mathrm{L}}$ and $E^{\upsilon}_{2,\mathrm{H}}$ are identified with ($D_{\alpha p}/2T^{**}$) and ($D_{\alpha p}/2T^{*}$) ($D_{\alpha p}$ is the parallel to D_C in eq 4), respectively. The amplitudes $A_{\upsilon,\mathrm{L}}$ and $A_{\upsilon,\mathrm{H}}$ are defined as

$$A_{\upsilon,\mathrm{L}} = -\frac{A_{\alpha p,\mathrm{L}}}{(1-\alpha)(T^{**})^{-\alpha}} \quad (7a)$$

$$A_{\upsilon,\mathrm{H}} = \frac{A_{\alpha p,\mathrm{H}}}{(1-\alpha)(T^{*})^{-\alpha}} \quad (7b)$$

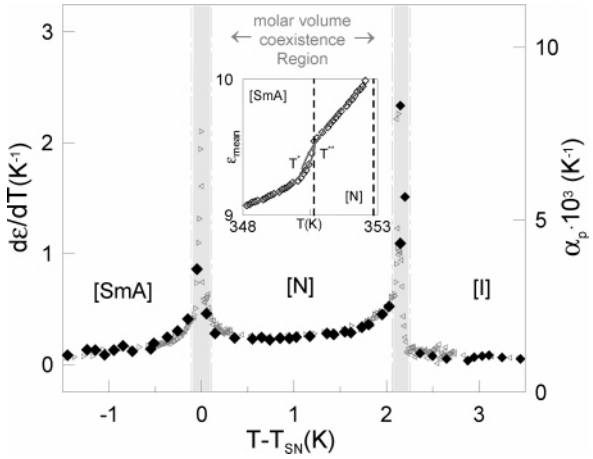

Figure 11. Derivative of the dielectric permittivity with temperature (black filled symbols) and thermal expansion coefficient data (gray open symbols) as a function of ($T - T_{SN}$) for 9OCB. The inset shows the behavior of the mean dielectric permittivity through the SmA-to-N transition. Grey solid lines are fittings according to equations such as eqs 6a and 6b. Shaded areas represent the molar volume coexistence region.

The results of fittings according to eq 6 of the ln υ data around the SmA-to-N phase transition are drawn in the inset of Figure 10A as well as consigned in Table 3. The extremely low value of the χ^2 values should be noticed. The amplitude ratio ($A_{\upsilon,\mathrm{S}}/A_{\upsilon,\mathrm{N}}$) through eq 7 correspond, in fact, to minus the ratio of amplitudes for the α_p data ($-A_{\alpha p,\mathrm{S}}/A_{\alpha p,\mathrm{N}} \approx 0.9$), which is close to that obtained from specific heat data ($A_{C,\mathrm{S}}/A_{C,\mathrm{N}} \approx 0.64$). Both T^* and T^{**} temperatures along with the volume transition temperature leading to ΔT^*, ΔT^{**}, and ($T^{**} - T^*$) values (see Table 1) are comparable to those reported from the specific heat determinations.

As for the α_p data around the N-to-I phase transition, the scaling with specific heat data is almost perfect, although a small discrepancy in the I phase, very close to the upper limit of the specific heat coexistence region, seems to exist. However, eqs 6a and 6b are assumed to portray well enough the experimental ln υ data, as indicated by the extremely low χ^2 values (Table 2) and as observed in the inset of Figure 10B, where both eqs 6 are drawn. The ratio of amplitudes ($A_{\upsilon,\mathrm{N}}/A_{\upsilon,\mathrm{I}}$) is found to be about −2.3, a value certainly very close to minus the amplitude ratio obtained from specific heat data. Again, but now at the N-to-I phase transition, the calculated ΔT^*, ΔT^{**}, and ($T^{**} - T^*$) values are comparable to those reported from the specific heat determinations (see Table 1).

Figure 11 shows α_p data, as an eye-guide, along with the derivative of the static permittivity data ($d\epsilon_{\mathrm{mean}}/dT$ and $d\epsilon_{\mathrm{iso}}/dT$) obtained by distortion-sensitive derivative analysis, as a function of ($T - T_{SN}$). It is quite obvious the existence of a scaling between both set of data, either dε/dT and α_p and so with specific heat data as well. Likewise, the existence of these scaling relationships allows one to try again the analysis of the static dielectric measurements around the SmA-to N phase transition using expressions similar to eq 6 to portray ϵ_{mean} data instead of eq 2. The results of the analysis are shown in the inset of Figure 11, where both equations of the same type as eq 6 are drawn. The fitting parameters have been consigned in Table 3, in which it seems to be good enough, as indicated by χ^2 values. It should be noted that, at the SmA side, the found independent term ($\epsilon^{**} = 9.52$) through eq 2b is comparable to that obtained from eq 6a ($E^{\epsilon}_{0,\mathrm{S}} = 9.533$), as well as both T^{**} temperatures, which are virtually the same. In addition, now the ratio of amplitudes ($A_{\epsilon,\mathrm{S}}/A_{\epsilon,\mathrm{N}}$) is found to be −0.7 instead

of −26, a value comparable to that reported from volumetric data ($A_{v,S}/A_{v,N} \approx -0.9$) and nearly identical in absolute value to the specific heat amplitude ratio.

4. Concluding Remarks

A thermodynamic description of both the SmA-to-N and N-to-I phase transitions of 9OCB compound through several physical magnitudes (dielectric, specific heat, and volumetric data) has been reported. Likewise, from dielectric determinations, in part devoted to the dielectric relaxation study, the molecular dynamics near phase transitions and in the SmA, N, and I phases has been investigated in detail. In such a relaxation study, performed in the frequency range from 10^2 to 1.8×10^9 Hz, two different alignments have been considered, parallel and perpendicular to the probing electric field. In the first one, molecular rotations around the short molecular axis (ω_1 mode) have been revealed as the most important contribution to the molecular dynamics and, in addition, the static dielectric permittivity around phase transitions has been proved to be strongly driven by this contribution. The perpendicular alignment leads to three contributions to the molecular dynamics, the most prominent being that corresponding to the precessional motion of the molecules around the director (ω_3 mode), although contributions of the other two modes (ω_4 and $\omega_{1\perp}$ modes) to the static dielectric permittivity, mainly around the N-to-I phase transition and in the N mesophase, have to be considered.

It has been experimentally proved that, around both phase transitions in 9OCB, α_p data, specific heat, and the derivative of the static dielectric permittivity (ϵ_{mean} and ϵ_{iso}) with temperature are related to each other by scaling relationships.

It has been found, irrespective the physical magnitude, that the N-to-I phase transition can be described by a specific heat critical exponent of about 0.5 (the tricritical value) in both the N and I sides. Likewise, on the N side, the order parameter critical exponent has been found to be 0.25 (the tricritical value as well). According to the Table 2, a comparable absolute value of the amplitude ratio (A_N/A_I) has been obtained, ranging between 2.3 (molar volume) and 2.9 (specific heat). As for ΔT^*, ΔT^{**}, and the width of the metastable N-to-I region ($T^{**} - T^*$), according to the Table 1, it seems to be slightly physically magnitude-dependent, as it was earlier reported by Anisimov[7] in the 1990s. In particular, ΔT^* and ($T^{**} - T^*$) values from dielectric determinations are too low as compared with the same transition in other liquid-crystal-like materials, but even so, they are twice of those found from specific heat and volumetric determinations, a fact which strongly supports the nearly tricritical character of the N-to-I phase transition in 9OCB. In addition, the ratio ($\Delta T^*/\Delta T^{**}$), irrespective of the technique, significantly differs from the theoretical L-dG value of 8, supposed to be universal.

It has been doubtless proved the first-order character of the SmA-to-N phase transition, very well described by means of the tricritical value of the specific heat critical exponent in both SmA and N sides ($\alpha_S = \alpha_N \approx 0.5$). In addition, the fittings of the static permittivity in both sides, according to equations of the same type as eq 6, lead to a comparable absolute value of the amplitude ratio ($A_S/A_N = 0.64-0.90$) as obtained by means of specific heat and volumetric determinations. From Table 1, although the value of ΔT^{**} is very low and nonphysically magnitude dependent, the value of ΔT^* found from dielectric measurements (0.58 K) is nearly 7 times higher than that reported from volumetric data and even 11 times higher than that reported from specific heat data. This discrepancy on ΔT^* and so on ($T^{**} - T^*$) between dielectric measurements on one side and specific heat and volumetric determinations on the other side was earlier observed for the N-to-I phase transition for other liquid crystals. However, for first-order SmA-to-N phase transitions, to the best of our knowledge, no evidence of such a discrepancy were reported in the past. In a similar way, as reported for the N-to-I phase transition, the ratio ($\Delta T^*/\Delta T^{**}$) for the SmA-to-N phase transition is also found to be far from the theoretical L-dG value.

It should be stressed that the width of the metastable region for the SmA-to-N transition is less than that found for the N-to-I transition, as expected for a weaker first-order phase transition of a nearly tricritical character. This fact can easily be extracted from the comparison of latent heats and volume jumps for both phase transitions. The coherence of such values has been tested through eq 5 using the measured $(dp/dT)_{SN}$ and $(dp/dT)_{NI}$ slopes at atmospheric pressure.

Acknowledgment. We are grateful for financial support from the MCYT of Spain (projects FIS2005-00975 and MAT2003-07806-C02-02), from the MEC (MAT2006-13571-C02-02), from the Generalitat de Catalunya (DURSI grant 2005SGR-00535), and from the Universidad del País Vasco (project 9/UPV060.310-13562/2001).

References and Notes

(1) Sied, M. B.; Salud, J.; López, D. O.; Barrio, M.; Tamarit, J. Ll. *Phys. Chem. Chem. Phys.* **2002**, *4*, 2587.
(2) Oweimreen, G. A.; Morsy, M. A. *Thermochim. Acta* **2000**, *346*, 37.
(3) Marynissen, H.; Thoen, J.; van Dael, W. *Mol. Cryst. Liq. Cryst.* **1983**, *97*, 149.
(4) Thoen, J.; Marynissen, H.; van Dael, W. *Phys. Rev. Lett.* **1984**, *52*, 204.
(5) Marynissen, H.; Thoen, J.; van Dael, W. *Mol. Cryst. Liq. Cryst.* **1985**, *124*, 195.
(6) Cladis, P. E.; van Saarloos, W.; Huse, D. A.; Patel, J. S.; Goodby, J. W.; Finn, P. L. *Phys. Rev. Lett.* **1989**, *62*, 1764.
(7) Anisimov, M. A.; Cladis, P. E.; Gorodetskii, E. E.; Huse, D. A.; Podneks, V. E.; Taratuta, V. G.; van Saarloos, W.; Voronov, V. P. *Phys. Rev. A* **1990**, *41*, 6749.
(8) Raja, V. N.; Prasad, S. K.; Rao, D. S. S.; Chandrasekhar, S. *Liq. Cryst.* **1992**, *12*, 239.
(9) Qian, S. H.; Iannacchione, G. S.; Finotello, D.; Steele, L. M.; Sokol, P. E. *Mol. Cryst. Liq. Cryst.* **1995**, *265*, 395.
(10) Cross, C. W.; Fung, B. M. *Liq. Cryst.* **1995**, *19*, 863.
(11) Qian, S. H.; Iannacchione, G. S.; Finotello, D. *Phys. Rev. E* **1996**, *53*, R4291.
(12) Mercuri, F.; Zammit, U.; Marinelli, M. *Phys. Rev. E* **1998**, *57*, 596.
(13) Marinelli, M.; Mercuri, F.; Zammit, U.; Scudieri, F. *Phys. Rev. E* **1998**, *58*, 5860.
(14) Marinelli, M.; Mercuri, F. *Phys. Rev. E* **2000**, *61*, 1616.
(15) Drozd-Rzoska, A.; Rzoska, S. J.; Ziolo, J. *Phys. Rev. E* **2000**, *61*, 5349.
(16) Bruno, V.; Scaramuzza, N.; Zammit, U. *Mol. Cryst. Liq. Cryst.* **2002**, *372*, 201.
(17) Jadzyn, J.; Czechowski, G.; Déjardin, J. L. *J. Phys.: Condens. Matter* **2006**, *18*, 1839.
(18) McMillan, W. L. *Phys. Rev. A* **1971**, *4*, 1238.
(19) Kobayashi, K. *Phys. Lett.* **1970**, *31A*, 125.
(20) de Gennes P. G.; Prost J. *The Physics of Liquid Crystals*; Oxford Science Publications: New York, 1994.
(21) Kumar S. *Liquid Crystals: Experimental Study of Physical Properties and Phase Transitions*; Cambridge University Press: New York, 2001.
(22) Marinelli, M.; Mercuri, F.; Zammit, U.; Scudieri, F. *Int. J. Thermophys.* **1998**, *19*, 595.
(23) Halperin, B. I.; Lubensky, T. C.; Ma, S. *Phys. Rev. Lett.* **1974**, *32*, 292.
(24) Halperin, B. I.; Lubensky, T. C. *Solid State Commun.* **1974**, *14*, 997.
(25) Tamblyn, N.; Oswald, P.; Miele, A.; Bechhoefer, J. *Phys. Rev. E* **1995**, *51*, 2223.
(26) Yethiraj, A.; Bechhoefer, J. *Phys. Rev. Lett.* **2000**, *84*, 3642.
(27) Yethiraj, A.; Mukhopadhyay, R.; Bechhoefer, J. *Phys. Rev. E* **2002**, *65*, 3642.
(28) Mukherjee, P. K.; Mukherjee, T. B. *Phys. Rev. B* **1995**, *52*, 9964.
(29) Mukherjee, P. K. *J. Phys.: Condens. Matter* **1998**, *10*, 9191.

(30) Keyes, P. H. *Phys. Lett. A* **1978**, 67, 132.
(31) Anisimov M. A. *Critical Phenomena in Liquids and Liquid Crystals*; Gordon and Breach Science Publishers: Amsterdam, 1991.
(32) Zywocinski, A. *J. Phys. Chem. B* **2003**, *107*, 9491.
(33) Thoen, J.; Marynissen, H.; van Dael, W. *Phys. Rev. A* **1982**, *26*, 2886.
(34) Drozd-Rzoska, A.; Rzoska, S. J.; Ziolo, J. *Phys. Rev. E* **1999**, *54*, 6452.
(35) Mukhopadhyay, R.; Mukherjee, P. K. *Int. J. Mod. Phys. B* **1997**, *11*, 3979.
(36) Mercuri, F.; Marinelli, M.; Zammit, U. *J. Therm. Anal.* **1998**, *52*, 739.
(37) Zywocinski, A.; Wieczorek, S. A. *Phys. Rev. A* **1985**, *31*, 479.
(38) Zywocinski, A.; Wieczorek, S. A. *J. Phys.Chem. B* **1997**, *101*, 6970.
(39) Pippard, A. B. *Philos. Mag.* **1956**, *1*, 473.
(40) Garland, C. W. *J. Chem. Phys.* **1964**, *41*, 1005.
(41) Mistura, L. *J. Chem.Phys.* **1973**, *59*, 4563.
(42) Rzoska, S. J.; Ziolo, J.; Sulkowski, W.; Jadzyn, J.; Czechowski, G. *Phys. Rev. E* **2001**, *64*, 052701.
(43) Sied, M. B.; López, D. O.; Tamarit, J. Ll.; Barrio, M. *Liq. Cryst.* **2002**, *29*, 57.
(44) Lafouresse, M. G.; Sied, M. B.; Allouchi, H.; López, D. O.; Salud, J.; Tamarit, J. Ll. *Chem. Phys. Lett.* **2003**, *376*, 188.
(45) Sied, M. B.; Salud, J.; López, D. O.; Allouchi, H.; Diez, S.; Tamarit, J. Ll. *J. Phys. Chem. B* **2003**, *107*, 7820.
(46) Puertas, R.; Rute, M. A.; Salud, J.; López, D. O.; Diez, S.; van Miltenburg, J. C.; Pardo, L. C.; Tamarit, J. Ll.; Barrio, M.; Pérez-Jubindo, M. A.; de la Fuente, M. R. *Phys. Rev. B* **2004**, *69*, 224202.
(47) Diez, S.; López, D. O.; De la Fuente, M. R.; Pérez-Jubindo, M. A.; Salud, J.; Tamarit, J. Ll. *J. Phys. Chem. B* **2005**, *109*, 23209.
(48) Diez, S.; Pérez-Jubindo, M. A.; De la Fuente, M. R.; López, D. O.; Salud, J.; Tamarit, J. Ll. *Chem. Phys. Lett.* **2006**, *423*, 463.
(49) Diez, S.; Pérez-Jubindo, M. A.; De la Fuente, M. R.; López, D. O.; Salud, J.; Tamarit, J. Ll. *Liq. Cryst.* **2006**, *33*, 1083.
(50) Zywocinski, A. *J. Phys. Chem. B* **1999**, *103*, 3087.
(51) Zywocinski, A.; Wieczorek, S. A.; Stecki, J. *Phys. Rev. A* **1987**, *36*, 1901.
(52) Nordio, P. L.; Rigatti, G.; Segre, U. *Mol. Phys.* **1973**, *25*, 129.
(53) Dunmur, D. A. and Urban S.; Würflinger A. In *Relaxation Phenomena: Liquid Crystals, Magnetic Systems, Polymers, High-T_c Superconductors, Metallic Glasses*; Haase, W., Wróbel, S., Eds.; Springer-Verlag: Berlin, 2003; p 163 (D.A.D.), p 181 (S.U.; A.W.).
(54) Jadzyn, J.; Czerkas, S.; Czechowski, G.; Burczyk, A.; Dabrowski, R. *Liq. Cryst.* **1999**, *26*, 437.
(55) Aliev, F. M.; Nazario, Z.; Sinha, G. P. *J. Non-Cryst. Solids* **2002**, *305*, 218.
(56) Leys, J.; Sinha, G.; Glorieux, C.; Thoen, J. *Phys. Rev. E* **2005**, *71*, 051709.
(57) Bose, T. K.; Campbell, B.; Yagihara, S.; Thoen, J. *Phys. Rev. A* **1987**, *36*, 5767.
(58) Williams, G. *The Molecular Dynamics of Liquid Crystals*; Luckhurst, G. R., Veracini, C. A., Eds.; Kluwer Academic Publishers: Norwell, MA, 1989; Chapter 17.
(59) Haws, C. M.; Clark, M. G.; Attard, G. S. *Side Chain Liquid Crystal Polymers*; McArdle, C., Ed.; Blackie: London, 1989; Chapter 7.
(60) Hill, N. E.; Vaughan, W. E.; Price, A. H.; Davies, M. *Dielectric Properties and Molecular Behaviour*; Van Nostrand Reinhold: New York, 1969; p 314.
(61) Maier, W.; Meier, G. *Z. Naturforsch.* **1961**, *16A*, 262.
(62) Drozd-Rzoska, A.; Rzoska, S. J.; Ziolo, J.; Jadzyn, J. *Phys. Rev. E* **2001**, *63*, 052701.
(63) Jadzyn, J.; Czechowski, G.; Legrand, C.; Douali, R. *Phys. Rev. E* **2003**, *67*, 041705.
(64) Iannacchione, G. S.; Finotello, D. *Phys. Rev. E* **1994**, 50, 4780.
(65) Kasting, G. B.; Lushington, K. J.; Garland, C. W. *Phys. Rev. B* 1980, *22*, 321.
(66) Islander, S. T.; Zimmermann, W., Jr. *Phys. Rev. A* **1973**, *7*, 188.
(67) Cusmin, P. Doctoral Thesis, Technical University of Catalonia, 2006; in preparation.